Characterization of lipidic markers of chondrogenic differentiation using mass spectrometry imaging

Beatriz Rocha[1], Berta Cillero-Pastor[2], Gert Eijkel [2], Anne L. Bruinen[2], Cristina Ruiz-Romero[1,3], Ron M. A. Heeren[2] and Francisco J. Blanco[1,4]

[1] Rheumatology Division, ProteoRed/ISCIII Proteomics Group, INIBIC – Hospital Universitario de A Coruña, A Coruña, Spain.

[2] Biomolecular Imaging Mass Spectrometry (BIMS), FOM Institute AMOLF, Amsterdam, The Netherlands.

[3] CIBER-BBN Instituto de Salud Carlos III, INIBIC-CHUAC, A Coruña, Spain.

[4] RIER-RED de Inflamación y Enfermedades Reumáticas, INIBIC-CHUAC, A Coruña, Spain.

*Address correspondence and reprint requests to:

Francisco J Blanco García (MD PhD)

INIBIC-Complejo Hospitalario Universitario A Coruña

C/ Xubias, 84, 15006-A Coruña (Spain)

Tel: 34-981-176399; Fax: 34-981-176398; E-mail address: fblagar@sergas.es

Abbreviations:

9-AA	9 aminoacridine
AA	Arachidonic acid
ASAH1	N-acylsphingosine amidohydrolase
Cer	Ceramide
DA	Discriminant analysis
DAG	Diacylglycerols
DHA	Docosahexaenoic acid
FA	Fatty acid
MAG	Monoacylglycerols
$[M+H]^+$	Singly protonated molecule
$[M+Na]^+$	Singly sodiated molecule
$[M+K]^+$	Singly potassiated molecule
$[M-H]^-$	Singly deprotonated molecule
MSI	Mass spectrometry imaging
PC	Phosphatidylcholine
PCA	Principal component analysis
PE	Phosphatidylethanolamine
PG	Phosphatidylglycerol
PI	Phosphatidylinositol
PLs	Phospholipids
Q-TOF	Quadrupole-time of flight
SIMS	Secondary ion mass spectrometry
SLs	Sphingolipids
SM	Sphingomyelin
SMPD1	Sphingomyelin phosphodiesterase 1
SPHK1	Sphingosine kinase 1
ST	Sulfatide

Keywords: Chondrogenesis, lipids, mass spectrometry imaging, mesenchymal stem cells, cartilage

Total number of words: 8384

Abstract

Mesenchymal stem cells (MSC) are an interesting alternative for cell-based therapy of cartilage defects attributable to their capacity to differentiate towards chondrocytes in the process termed chondrogenesis. The metabolism of lipids has recently been associated with the modulation of chondrogenesis and also with the development of pathologies related to cartilage degeneration. Information about the distribution and modulation of lipids during chondrogenesis could provide a panel of putative chondrogenic markers. Thus, the discovery of new lipid chondrogenic markers could be highly valuable for improving MSC-based cartilage therapies. In this work, mass spectrometry imaging (MSI) was used to characterize the spatial distribution of lipids in human bone marrow MSCs (hBMSCs) during the first steps of chondrogenic differentiation. The analysis of MSC micromasses at days 2 and 14 of chondrogenesis by matrix-assisted laser desorption ionization-mass spectrometry imaging (MALDI-MSI) led to the identification of 20 different lipid species, including fatty acids (FA), sphingolipids (SLs) and phospholipids (PLs). Phosphocholine, several sphingomyelins (SMs) and phosphatidylcholines (PCs) were found to increase during the undifferentiated chondrogenic stage. A particularly detected lipid profile was verified by time-of-flight secondary ion mass spectrometry (TOF-SIMS). Using this technology, a higher intensity of phosphocholine-related ions was observed in the peripheral region of the micromasses collected at day 14.

1. Introduction

Mesenchymal stem cells (MSCs) are adult stem cells that have unique properties of self-renewal, proliferation and potential for multilineage differentiation [1]. Although MSCs can be isolated from various adult mesenchymal tissues, currently they are typically extracted from bone marrow (BMSCs) or umbilical cords, and subsequently induced to differentiate into cell types, such as adipocytes, osteoblasts, and chondrocytes [2]. Chondrogenesis is the process by which MSCs differentiate towards chondrocytes and begin secreting the molecules that form the cartilage extracellular matrix (ECM) [3]. Because of their chondrogenic potential, MSCs have been recognized as promising candidates for cell-based therapies of cartilage defects [4].

Chondrogenesis includes mesenchymal cell condensation and chondrocyte differentiation, processes that are induced by the culture of MSCs in three-dimensional, high density aggregates (pellet or micromass culture) [5] with factors, such as transforming growth factor β (TGFβ) [6]. The presence of these factors is one of the earliest signals in chondrogenic condensation [7]. Models of chondrogenesis based on BMSCs have been developed and characterized in an attempt to promote cell therapy-based strategies of cartilage repair [4, 5]. However, the lack of knowledge on the precise molecular mechanisms participating in this differentiation process, as well as the absence of well-defined markers for chondrogenesis, have hindered achievement of satisfactory results [8].

Recent studies have highlighted the importance of lipid metabolism in the modulation of chondrogenesis. For example, the role of cholesterol in the regulation of growth plate chondrogenesis [9] and skeletal development [10] was recently established. Other studies found a positive effect of acid ceramidase (an essential compound to maintain the metabolic balance of several important bioactive lipids, such as ceramide or sphingosine) on the

chondrogenesis of bone marrow-derived mesenchymal stem cells (BMSCs) [11]. Other reports indicate that there is a close association between altered lipid metabolism and cartilage degenerative diseases, such as osteoarthritis (OA) [12], which has recently been found to be related to hypercholesterolemia [13] and altered levels of phospholipids in the synovial fluid [14]. Thus, the global analysis of lipidic modulations during chondrogenesis might provide important information on the molecular mechanisms participating in this process.

The large-scale study of lipids, lipidomics, has captured the attention of the scientific community in recent years because of the potential value of its use for discovery of novel biomarkers, signalling pathway relationships or disease molecular mechanisms [15, 16]. Technological progress has also facilitated the emergence of this new field of research, providing innovative possibilities for the structural analysis of lipids and their role in cellular metabolism. Mass spectrometry imaging (MSI) is a high-throughput technique for determining and visualizing the spatial distribution of biomolecules in thin tissue sections [17]. Direct MSI analyses of tissue sections can obtain biomolecular profiles from very small samples with little tissue disruption. These techniques include matrix-assisted laser desorption ionization (MALDI), secondary ion mass spectrometry (SIMS), desorption electrospray ionization (DESI), and others.

In the present study, we employed both MALDI-MSI and time-of-flight secondary ion mass spectrometry (TOF-SIMS) for the identification and localization of lipids in a model of chondrogenesis developed in our laboratory [18]. This model of three-dimensional human BMSC cultures (micromasses) has recently shown potential usefulness to promote repair of articular cartilage defects in a cell therapy-based strategy [19]. We had already performed a comprehensive analysis of the intracellular and extracellular protein modulations in this model at days 2 and 14 of chondrogenesis [20, 21]. The further definition of characteristic

differential lipidic profiles in this model of chondrogenesis will be valuable for the discovery of novel markers of chondrogenesis.

2. Materials and Methods

2.1. Chemicals and materials. Gelatin, α-cyano-4-hydroxycinnamic acid (CHCA), 9-aminoacridine (9-AA) and polyethylene glycol (PEG) were purchased from Sigma-Aldrich (Munich, Germany). Water, acetonitrile (ACN), ethanol, methanol and trifluoroacetic acid (TFA) were purchased from Biosolve (Valkenswaard, The Netherlands).

2.2. Samples procurement and processing. Bone marrow samples were obtained as trabecular bone biopsy specimens from femoral heads of consenting donors undergoing total hip replacement at the Complejo Hospitalario Universitario A Coruña. The study was approved by the Ethics Committee of Galicia. Human BMSCs (hBMSCs) isolated from three donors (68-84 years-old) were used for this study. Following hBMSCs isolation and expansion, chondrogenic differentiation was achieved using the previously described micromass three-dimensional culture system [20]. Micromasses were collected at 2 and 14 days of chondrogenic differentiation and embedded in 10% gelatin. Samples were then cut into 10 µm thickness sections using a cryostat (Leica Microsystems, Barcelona, SP) and placed on conventional microscope slides for MALDI imaging or on 25 mm x 50 mm x 1.1 mm indium tin oxide (ITO) high conductivity slides (Delta Technologies, CO, USA) with a specific surface resistance of 4-8 Ω for TOF-SIMS measurements. The slides were then stored at -20ºC until further analysis. Two sections of micromasses for each time-point of chondrogenesis from each of three donors were analyzed in both positive and negative ion approaches by MALDI-MSI. TOF-SIMS experiments were performed in the positive ion mode.

2.3. Matrix application. Before matrix application, slides were first placed in a desiccator box at 4ºC and defrosted for 10 min, and then placed inside a vacuum desiccator at room temperature (RT) for 20 min to prevent molecular delocalization. For positive ion mode MALDI-MSI experiments, CHCA matrix solution was prepared at 10 mg/ml in 70% methanol and 30% H_2O containing 0.2% TFA. A 9-AA matrix solution at a final concentration of 10 mg/ml was prepared in 70% ethanol and 30% H_2O and used for the negative ion mode MALDI-MSI analysis. Micromass sections were homogeneously covered by the matrix solution using a vibrational sprayer (ImagePrep; Bruker Daltonics, Bremen, Germany). Briefly, the coating step consisted of 45 cycles was repeated three times. Each cycle contained three phases in which a matrix layer was added by a spray of 20 s followed by 20 s of incubation time and 30 s of drying time (influx of nitrogen). The glass slide was turned 180º after each coating step of 45 cycles.

2.4. MALDI-MSI. Tissue sections were optically scanned prior to MALDI-MSI experiments using a 2400 dots per inch desktop scanner (HP, Hewlett-Packard, Palo Alto, CA, USA). The resulting images were imported into the MALDI Imaging Pattern Creator software (Waters Corporation, Manchester, UK). The samples were then analyzed by a MALDI-Q-TOF SYNAPT HDMS instrument (Waters) equipped with a 200-Hz Nd:YAG laser. The data were acquired in the positive and negative V-reflectron mode with a 100 µm x 100 µm raster size (100 µm pixel size), within the 100-1000 mass/charge (m/z) range. Instrument calibration was performed using a standard calibration mixture of polyethylene glycol (PEG) (An equimolar mixture of PEG 100, PEG 400, PEG 1000, PEG 1500, PEG 2000 and PEG 3000, Sigma-Aldrich, St. Louis, Missouri, USA) with a MW range of 100-3000 Da. Data were visualized using Biomap 3.7.5.5 software (Novartis Pharma, Basel, Switzerland). Mass Spectrometry (MS) data were normalized according to the total ion current per spectrum

(TIC) to eliminate variations in the ionization efficiency or matrix deposition. Peak average intensities were calculated for each mass of interest.

2.5. Multivariate statistical analysis and data interpretation following MALDI-MSI. Principal components analysis (PCA) and discriminant analysis (DA), were used to search for spectral similarities and differences between the samples using an in-house built ChemoneTricks toolbox for MATLAB version 2011b (The MathWorks, Natick, Massachusetts). The MS raw data were first converted to the MATLAB format, followed by spectral binning to 0.1 Da bins for MALDI and 0.05 Da bins for TOF-SIMS. Peak picking was performed with the in-house built PEAPI software [22]. DA was performed employing the double stage PCA approach [23]. All on-pellet spectra were included in the analysis. The number of principal components used as input for DA for MALDI was limited to one quarter of the total number spectra to prevent overfitting of the DA model. For TOF-SIMS the highest ranked principal components that account for 80% of the variance where selected as input for DA. DA was utilized to select the peaks with the highest differences between the micromasses at day 2 and 14 of chondrogenesis. A specific group number (1 for day 2 samples and 2 for day 14 samples) was assigned to the spectra from each time of chondrogenesis. DA was performed on this data. To determine the reproducibility on a per donor level, a second group layout was created in which the spectra from each individual donor/day combination where assigned an unique group number (donor1 day2: group 1; donor1 day2: group 2; donor2 day2: group 3 etc.). After data analysis, m/z values of interest were selected for further identification.

2.6. Lipid identification by tandem mass spectrometry (MS/MS) analysis. Lipid identification was performed in both positive and negative ion modes using a MALDI-Q-TOF SYNAPT HDMS system (Waters) after completing MALDI-MSI experiments on different micromass slices. Lipid ion precursors were selected within a 1 Da selection window and fragmented using 20-30 V collision energy applied in the trap cell. The obtained spectra were processed using MassLynx software (Waters). The MS/MS fragmentation pattern from each selected mass was used to identify the lipids of interest and to assign them to previously classified lipid-m/z identifications in the LIPID Metabolites and Pathways Strategy Structure Database (LMSD) www.lipidmaps.org, and from relevant literature.

2.7. TOF-SIMS acquisition and processing. Slides were defrosted and dried in a vacuum desiccator at RT for 20 min, followed by gold coating using a Quorum Technologies (Newhaven East Sussex, UK) SC7460 sputter coater equipped with a FT707 quartz crystal microbalance stage and a FT690 film thickness monitor to deposit a 2 nm gold layer. TOF-SIMS experiments were performed on a Physical Electronics TRIFTII (Eden Prairie, Minnesota, USA) time of flight secondary ion mass spectrometer (TOF-SIMS) equipped with a 22KeV energy (2-3 nA) current Au^{1+} primary ion beam. Image areas of 1.8 mm x 1.8 mm were acquired as a mosaic of 32 x 32 tiles, each containing 256 x 256 pixels. The raster size was set at 56 µm and the acquisition time was 63.8 s per tile. The data were visualized using WinCandence software version 4.4.0.17 (Physical Electronics, Chanhassan, MN, USA).

2.8 Real-Time PCR assays. Total RNA from MSC pellet cultures at 2 and 14 days was extracted using the Trizol L.S. reagent (Invitrogen, Madrid, Spain), according to the manufacturer`s instructions. Between three and five micromasses per donor were employed for this analysis. A total of 1 µg RNA was used for the first-strand complementary DNA (cDNA) synthesis using the SuperScript® VILO cDNA Synthesis kit (Life Technologies).

The reverse transcription (RT) reaction was performed in a 10 µl reaction volume containing SuperScript® VILO™ Mastermix (2 µl) and the RNA (8 µl) at 25ºC for 10 minutes, followed by 60 minutes at 42ºC and 5 minutes at 85ºC to inactivate the enzyme. Quantitative real-time PCR was performed to assess the expression of the three enzymes involved in sphingomyelin metabolism (SMPD1, ASAH1 and SPHK1). All reactions were performed in 96-well plates using the LightCycler 480 instrument (Roche, Basel, Switzerland). The reaction was carried out in a 20 µl total volume containing 10 µl of the LightCycler® 480 Probes Master, 2.5 µl of the RT reaction mixture, 0.7 µl (20 µM) of each primer, 0.2 µl of probe (10 µM) and 5.9 µl of water. The PCR program consisted of initial pre-incubation for activation of FastStart Taq DNA Polymerase and denaturation of DNA at 95ºC for 10 min, followed by 50 cycles of at 95ºC for 10 s, annealing at 60ºC for 30 s, and extension at 72ºC for 1 s. Primers for SMPD1, ASAH1, SPHK1 and RPL13A (housekeeping gene) were designed using the Universal Probe Library tool available at the Roche website (http://www.roche-applied-science.com). Calculation of the normalized relative expression levels at the two times points of chondrogenesis (14 days vs. 2 days) was done using the qbasePLUS software version 1.5 (Biogazelle, Zwijnaarde, Belgium). Normalization was carried out with the stably expressed ribosomal reference gene RPL13A validated using the genormPLUS module in qbasePLUS.

3. Results

3.1. Positive MALDI-MSI analysis of the lipid composition of hBMSCs at days 2 and 14 of chondrogenesis.

The experimental workflow followed in this work for the characterization of lipids in hBMSCs micromasses at different time points of chondrogenesis is described in Supplementary Figure 1.

As indicated, we first analyzed the lipid composition of hBMSCs using MALDI-MSI in the positive ion mode. Thin micromass sections obtained from three patients were studied in duplicate. 683 spectra acquired in the mass range 100 to 1000 Da were analyzed by PCA and DA. As illustrated in the frequency plot of Figure 1A, the first discriminant function (DF1) separated the data into two groups corresponding to day 2 and day 14 of chondrogenesis. The discriminant loading spectra for Figure 1A displayed specific masses at each time point (Figure 1B). The positive fraction of masses indicated the specific molecular profile expressed at day 14 of chondrogenesis, whereas the peaks of the negative fraction were specific for the micromasses collected at day 2. The negative part of the graph was mainly dominated by many peaks with a high loading in the mass range of 600 to 900, such as m/z 682.5, m/z 739.5 and m/z 798.5, at which the phospholipids (PLs) and sphingolipids (SLs) are typically visualized by MALDI-MSI. In the low mass range we observed some other specific peaks as major discriminating masses from the negative fraction, such as choline at m/z 104.1, phosphate-related ions at m/z 146.9 and 162.9, phosphocholine at m/z 184.1, and a phosphocholine-related ion at m/z 198.1. On the other hand, positive loading spectra revealed a low lipid signal. In fact, only the masses m/z 729.5, m/z 790.5 and m/z 832.5 were specific of day 14 samples. Statistical analyses were performed on the three biological replicates independently and achieved highly reproducible results among donors (Supplementary Figure 2).

3.2. Negative MALDI-MSI analysis of the lipid composition of hBMSCs at days 2 and 14 of chondrogenesis.

Ion suppression in MALDI-MSI is a well-known process demonstrated among lipid classes. In fact, phosphatidylcholines (PCs) and sphingomyelins (SMs) can prevent the detection of other phospholipids present in the sample when using the positive ion mode. Aside from that, many lipids, including some classes of phospholipids and acidic

sphingolipids (sulfatides), preferentially ionize in the negative ion mode [24]. For this reason, micromass sections were also assessed in the negative ion mode by MALDI-MSI. A total of 745 spectra were analyzed by the statistical methods mentioned above. After DA, two groups corresponding to the undifferentiated and differentiated stage were clearly distinguishable in the negative ion mode. Moreover, DF1 scores had a different distribution in day 2 and day 14 samples; this indicates a characteristic lipid profile for each chondrogenic time point (Figure 1C). The DF1 spectrum revealed specific masses from day 2 (positive loadings) and day 14 micromasses (negative loadings) (Figure 1D). Some examples of 14 day-specific peaks were unsaturated fatty acids (FA) such as m/z 303.2 corresponding to arachidonic acid (AA) (C20:4) and m/z 327.2 linked to ω-3 docosahexaenoic acid (DHA) (C22:6). Other masses detected in the mass range of phospholipids (600-900), m/z 750.5, m/z 819.5 and m/z 885.6, also increased in the micromasses collected at day 14 according to the DA. On the other hand, several peaks specifically increasing at day 2 of chondrogenesis, m/z 323.0, m/z 403.0 and m/z 606.1, represent new markers of the undifferentiated stage.

3.3. Visualization of lipid distribution in hBMSCs at days 2 and 14 of chondrogenesis.

The intensity and the spatial distribution of the lipid species recorded by MALDI-MSI in the micromasses collected at days 2 and 14 of chondrogenesis were examined using Biomap software (Figure 2). First, we imaged some of the positive ion peaks obtained after doing the DA in days 2 and 14 samples (Figure 2A) and observed a difference in the normalized intensity of these peaks. For example, we observed higher intensities of phosphocholine (m/z 184.1) and some SM fragments, such as m/z 542.5 and m/z 666.5, in the micromasses collected on day 2. The PC signals at m/z 782.6, m/z 824.6 and m/z 826.6 showed the same pattern of differences when days 2 and 14 samples were compared. The distribution and intensities of all the identified lipid species in the positive ion mode are summarized in Supplementary Figure 3. In addition, 10 negative lipid species were also visualized in the two

conditions (Figure 2B). In these cases, the intensity of m/z values corresponding to AA (m/z 303.2) and DHA (m/z 327.2) was higher in the micromasses collected at day 14 than in the day 2 samples. This analysis also confirmed the predominant expression of the PLs, m/z 750.5, m/z 794.5, m/z 883.6 and 943.5, at day 14 of chondrogenesis.

However, the different distributions of positive lipid species and negative lipid species did not allow us to characterize specific inner areas within the micromass sections.

3.4. Structural characterization of lipid ions by tandem mass spectrometry revealed a differential lipid profile in hBMSCs during chondrogenesis.

After statistical analysis, the m/z values with the highest loadings were selected for identification of the lipid structure. MALDI-MS/MS profiling experiments were performed directly on the micromass sections under the experimental conditions described in Materials and Methods. The lipid assignment for each selected peak and the chondrogenic time point at which it was mainly expressed are summarized in Table 1. The m/z values in Table 1 are listed in order of their mass range. The assignment of m/z values was based on the bibliography and the Lipidmaps.org database. Contrary to the positive ion mode, where lipids can be protonated ($[M+H]^+$) or cationized by sodium ($[M+Na]^+$) or potassium ($[M+K]^+$), the negative mode mainly leads to the detection of deprotonated $[M-H]^-$ ion species, allowing easier attribution of lipids.

In total, 37 ion peaks were identified in positive and negative ion modes. Most of the ion peaks detected in the positive ion mode were attributable to PC and SM lipid classes. Six different PC species were identified. With the exception of m/z 790.5 [related to PC (C18:0/C18:0)] and m/z 832.5 [corresponding to PC (C18:0/C20:4)] that were increased at day 14 of chondrogenesis, all PC masses were more abundant in day 2 samples. Among the five different indentified SMs, only SM (d18:1/18:1), detected at m/z 729.5, was 14 day-specific. In addition to the intact lipid species, four fragments of PC (C16:0/C18:1) and two

fragments of SM (d18:1/C16:0) were identified. Other peaks, like phosphocholine (m/z 184.1) and a phosphocholine-related ion (m/z 198.1), were also increased in the micromasses collected at day 2, as mentioned above. Supplementary Figure 4A presents the MS/MS spectrum of m/z 725.5, already assigned to SM d18:1/C16:0 [25], obtained after the positive-profiling experiments. The collision-induced dissociation (CID) spectrum of this precursor showed three characteristic fragment ion signals at m/z 264.3, m/z 542.5 and m/z 666.5. The m/z 264.3 fragment ion corresponds to sphingosine base, whereas the m/z 542.5 and m/z 666.5 correspond to the loss of phosphocholine (184 Da) and trimethylamine (59 Da) from the SM precursor. The product ion spectrum of the precursor ion m/z 739.5 (Supplementary Figure 4B) was also recorded on the micromass sections. In the negative ion mode, 11 different ion peaks were identified by the MALDI-MS/MS measurements. Almost all were predominantly expressed in the micromasses collected at day 14 and were mainly attributed to the PI and PE lipid classes. The ions m/z 750.5 and m/z 794.5 belong to PEs, whereas the signals at m/z 883.6, m/z 885.6 and m/z 943.5 correspond to PIs. The ion peak m/z 778.5 is attributable to a sulfatide (ST) while that of m/z 819.5 is a phosphatidylglycerol (PG) (Table 1). Supplementary Figure 4C shows the fragment ion spectrum of m/z 819.5 (PG C18:1/C22:6) obtained after profiling in the negative ion experiments. The assignment of the FA chain lengths was confirmed by the signals at m/z 281.2, which corresponds to oleic acid (C18:1), and m/z 327.2 attributable to DHA (C22:6). Finally, dehydrated phosphoglycerol (m/z 153), a fragment ion commonly found in PLs, was detected. The identification of the m/z 885.6 precursor ion is shown in Supplementary Figure 4D. The mass peaks of m/z 241 and m/z 223 confirm the presence of the phosphoinositol head group, whereas the m/z 283 and m/z 303 fragment ions correspond to the stearic FA (C18:0) and arachidonic FA (C20:4), respectively. The assignment of the FA chain lengths was confirmed by the ion peaks m/z

581 and m/z 601. Finally, the fragment ion at m/z 419 is related to the loss of the inositol head group (162 Da) plus the FA C20:4 chain.

3.5. Differential lipid profiles by TOF-SIMS analysis of hBMSCs at days 2 and 14 of chondrogenesis.

Traditional TOF-SIMS instruments have limited mass resolution, lack of sensitivity to detect compounds (or metabolites) within the mass range over 1000 Da and they are incompatible with tandem MS analyses. However, recent progress in TOF-SIMS instrumentation has developed modern TOF-SIMS with MS/MS capabilities [26, 27]. SIMS is a unique tool for high spatial resolution MSI of elements and small organic molecules on biological tissues [28]. For this reason and because of the differences in ionization could give extra information on the molecular profiles, we decided to analyze the micromass sections by using this technology. After TOF-SIMS measurements in the positive ion mode, PCA and DA were applied to ascertain the specific masses differentially expressed between the two time points analyzed. The lipid profile of hBMSCs obtained by statistical analysis is shown in Table 2. Notably, we were able to validate a group of lipids, also found by MALDI-MSI, mostly increased at day 2: including phosphocholine, some lipid fragments (m/z 504.3, m/z 542.5 and m/z 666.5) and some PC and SM species (m/z 682.5, m/z 782.6, m/z 824.5 and m/z 826.6) previously detected by MALDI-MSI. In addition, we found an important number of m/z values in the mass range of 300 to 600. All of these were predominantly expressed in the differentiation stage and were mainly attributable to monoacylglycerols (m/z 313.4, m/z 339.4 and m/z 341.4), diacylglycerols (DAGs) (m/z 551.6, m/z 575.7, m/z 579.7, m/z 603.7, m/z 605.7 and m/z 607.8) and ceramide lipid classes (m/z 576.7 and m/z 604.8).

3.6. Different localization of phosphocholine-related ions.

Several attempts have been made to improve the spatial resolution of MALDI imaging, including oversampling [29], laser modulation [30] and solvent-free sublimation matrix application techniques [31]. In fact, MALDI-MSI instrumentation can usually achieve a spatial resolution of 10 μm [32]. In addition, detailed information on lipids in different anatomical areas of tissues can be obtained by MALDI-MSI, although single cell or intracellular assessments can not be performed. In our study, the localization of the lipid ions after MALDI-MSI measurements was similar in micromasses collected at days 2 and 14 of chondrogenesis; we were unable to detect lipid ions with a different distribution profile between the samples, primarily because of the small size of the micromasses (1-2 mm).

SIMS is utilized for very high spatial resolution MSI, as mentioned above. In fact, the lateral resolution of TOF-SIMS can be less than 1 μm [33]. Therefore, the application of TOF-SIMS could reveal some variations in the lipid localization between the two time points of chondrogenesis. The choline signal (m/z 104.1) and the phosphocholine (m/z 184.1) signals, measured in the positive ion mode, were homogeneously distributed in the membrane of the cells throughout the micromass sections at day 2 (Figure 3). However, in the micromasses collected at day 14, phosphocholine-related ions were more abundant in the peripheral cells, suggesting a more advanced differentiation of the cells situated in the micromass core. This analysis showed the intrasample heterogeneity in the 14 days samples.

3.7. SPHK1 expression is increased at day 14 of chondrogenesis.

To further investigate the low detection of SMs intact species in the micromasses of hBMSCs undergoing chondrogenesis, we performed real-time PCR analyses on samples from six independent differentiation experiments using hBMSCs of additional donors, at days 2 and 14. The analyses included the quantitative assessment of gene expression of three enzymes involved in the SM metabolism (Figure 4), such as sphingomyelin

phosphodiesterase 1 (SMPD1, responsible for cleaving SM into phosphocholine and ceramide), N-acylsphingosine amidohydrolase or acid ceramidase 1 (ASAH1, involved in the generation of sphingosine from ceramide), and sphingosine kinase 1 [SPHK1, which phosphorylates sphingosine to sphingosine-1-phosphate (S1P)]. As shown in Figure 4, a clear up-regulation (4.74-fold) was found for SPHK1 ($p<0.05$) at day 14 when compared to day 2. Up-regulations of ASAH1 and SMPD1 were also detected, although in these cases the results showed a tendency, but were not significant ($p<0.1$). Taken together, these data suggest an increased activity of this pathway, which might enhance SM degradation during chondrogenesis.

4. Discussion

Among the different mass spectrometry imaging techniques, MALDI-MSI is the highest performing MSI tool currently available in terms of sensitivity for intact biomolecules and mass range. It has rapidly developed in the biomedical field, particularly in the investigation of tissues from colon [34], breast [35] and prostate [36] cancers. Investigating rheumatology disorders, MALDI-MSI has been recently employed for the study of osteoarthritic (OA) cartilage [37, 38]. An alternative technique, TOF-SIMS, provides better spatial resolution than MALDI and its application in the biomedical field has also been capitalized upon [39]. As with MALDI, healthy and OA cartilages have been also subjected to TOF-SIMS analysis, the results of which has specifically localized cholesterol and FAs in the superficial area of OA tissue [40]. In the present study, we combined these two MSI technologies to analyze the lipid distribution of MSCs during chondrogenic differentiation.

The distribution of lipids has previously been examined in adipose [41], bone [42] and cartilage [40] tissues using MSI technologies. Given the potential of these tools for gaining a better understanding of basic biology, MSI has also been increasingly applied in stem cell

research. For example, multi-isotope imaging mass spectrometry (MIMS) and TOF-SIMS have been employed to quantify stem cell division and metabolism in mice [43], and to characterize the distribution of strontium during the osteogenic differentiation of MSCs [44], respectively. However, to date, no MSI studies have specifically focused on those lipid modulations occurring during differentiation of MSCs towards chondrocytes, which have been reported to alter the chondrogenic phenotype [11], and to be essential for proper cartilage formation [9, 10]. This lack emphasizes the importance of studies on lipid modulations to better our understanding of the molecular processes that drive chondrogenesis.

Therefore, for the first time, we applied MSI technologies to characterize the lipid profile of hBMSCs during the early stages of chondrogenic differentiation. Among the lipid classes identified by MALDI-MSI, phosphatidylcholines (PCs) and sphingomyelins (SMs) levels decreased during chondrogenic differentiation. Apart from their role as structural components of plasma membranes, the products of SM metabolism, such as ceramides, sphingosine, S1P and DAGs, function as cellular signaling molecules, participating in cell growth, cell differentiation and programmed cell death [45]. Thus, our data indicate that, during chondrogenesis, hBMSCs mobilize the SMs to produce the secondary metabolites necessary for differentiation towards chondrocytes. In addition, we found a significantly higher expression of the enzyme SPHK1 at day 14 compared with day 2 of chondrogenesis, this explains the low level of identification of intact SM species at day 14. The use of TOF-SIMS also enabled the detection of the presence of some PC (m/z 782.6, m/z 824.5 and m/z 826.6) and SM fragments (m/z 542.5 and m/z 666.5) characteristic of the early stages of chondrogenesis. Moreover, TOF-SIMS analysis revealed the presence of some ceramide lipid species (m/z 576.7 and m/z 604.8) in the micromasses collected at day 14. The effect of ceramide on mesenchymal stem cell differentiation, such as adipogenesis [46] and

chondrogenesis [11] has been already studied. The detection of ceramide correlates with the drop of SM levels at day 14 of chondrogenesis. For these reasons, the loss of SMs during chondrogenesis may be used as a novel chondrogenic marker.

In addition, phosphocholine was preferentially identified at day 2 by both MSI techniques. Phosphocholine represents choline storage *in vivo* and is related to the size of the cell membrane [47]. We hypothesize that, after 14 days of chondrogenesis, the resulting chondrocyte-differentiating hBMSCs are smaller in size than non-induced hBMSCs because, during chondrogenesis, hBMSCs stop proliferating to begin differentiation into chondrocytes. Therefore, the decreased levels of phosphocholine during chondrogenesis could induce the synthesis of inositol- and ethanolamine-derived PLs that were detected by MALDI-MSI at day 14 of chondrogenic differentiation. Moreover, TOF-SIMS measurements indicate that phosphocholine-related ions are specifically localized in the peripheral cells of the micromasses collected at day 14. These analyses showed the intrasample heterogeneity in the 2 and 14 days samples. In addition, some of the masses increased at day 14 detected by TOF-SIMS, such as m/z 551.6 (DAG) and m/z 578.7 (not identified) were localized in the core of the 14 days micromasses (data not shown). These facts points to a higher level of chondrogenic differentiation in the core of the 3D structures where there is a lower availability of oxygen. This observation demonstrates the capability of TOF-SIMS to discriminate with high spatial resolution the different stages of chondrogenesis. Following the same principle that we used for MALDI-MSI, samples were also grouped by donor after TOF-SIMS experiments, observing that DF3 showed the differences between the two time points being able to discriminate between different donors attending to the DF scores (data not shown). Therefore by looking at the different DFs we could obtain information about the state of chondrogenesis, lipid profiles and link this data with the respective donor. This

methodology could provide valuable information to select the best conditions/donors for cell therapy strategies in the future.

Overall, we have described for the first time the lipid changes from hBMSCs in their early stages of chondrogenic differentiation. Accumulation of sphingomyelin was detected in the undifferentiated stage using MALDI-MSI. Moreover, TOF-SIMS revealed a higher abundance of phosphocholine-related ions in the peripheral cells of day 2-related micromasses. These results demonstrate that MSI is a useful tool to discriminate different areas of the micromasses and to understand the molecular processes that occur during the differentiation of hBMSCs towards chondrocytes and/or cartilage-like tissues. Furthermore, these molecules may have key functional roles in chondrogenesis and could be candidate chondrogenic differentiation markers. Therefore, these lipids could have potential value in cartilage reparation strategies.

Acknowledgements

The authors express appreciation to the Pathology Service from the Orthopaedics Department of the CHU A Coruña for providing bone marrow samples, to Tamara Hermida and Maria José Sánchez for hBMSCs isolation and characterization, and to Purificación Filgueira and Noa Goyanes for obtaining the micromass sections. B. Rocha and C. Ruiz-Romero are recipients of grants from ISCIII-Spain (PFIS and Miguel Servet, respectively). This work was supported in part through funding from EU COST Action BM1104 (Mass Spectrometry Imaging: new tools for healthcare research), and also from Fondo Investigación Sanitaria, Madrid, Spain (CIBER-CB06/01/0040; PI12/00329; PI11/02397, RETIC-RIER-RD12/0009/0018; Proteo-Red/ISCIII); FEDER (European Community) and Xunta de Galicia (Red Gallega REDICENT).

5. References

[1] Koga, H., Engebretsen, L., Brinchmann, J. E., Muneta, T., Sekiya, I., Mesenchymal stem cell-based therapy for cartilage repair: a review. *Knee Surg Sports Traumatol Arthrosc* 2009, *17*, 1289-1297.

[2] Pittenger, M. F., Mesenchymal stem cells from adult bone marrow. *Methods Mol Biol* 2008, *449*, 27-44.

[3] Goldring, M. B., Tsuchimochi, K., Ijiri, K., The control of chondrogenesis. *J Cell Biochem* 2006, *97*, 33-44.

[4] Gupta, P. K., Das, A. K., Chullikana, A., Majumdar, A. S., Mesenchymal stem cells for cartilage repair in osteoarthritis. *Stem Cell Res Ther* 2012, *3*, 25.

[5] Johnstone, B., Hering, T. M., Caplan, A. I., Goldberg, V. M., Yoo, J. U., In vitro chondrogenesis of bone marrow-derived mesenchymal progenitor cells. *Exp Cell Res* 1998, *238*, 265-272.

[6] Spagnoli, A., O'Rear, L., Chandler, R. L., Granero-Molto, F., *et al.*, TGF-beta signaling is essential for joint morphogenesis. *J Cell Biol* 2007, *177*, 1105-1117.

[7] Tuli, R., Tuli, S., Nandi, S., Huang, X., *et al.*, Transforming growth factor-beta-mediated chondrogenesis of human mesenchymal progenitor cells involves N-cadherin and mitogen-activated protein kinase and Wnt signaling cross-talk. *J Biol Chem* 2003, *278*, 41227-41236.

[8] Huey, D. J., Hu, J. C., Athanasiou, K. A., Unlike bone, cartilage regeneration remains elusive. *Science* 2012, *338*, 917-921.

[9] Wu, S., De Luca, F., Role of cholesterol in the regulation of growth plate chondrogenesis and longitudinal bone growth. *J Biol Chem* 2004, *279*, 4642-4647.

[10] Schmidt, K., Hughes, C., Chudek, J. A., Goodyear, S. R., *et al.*, Cholesterol metabolism: the main pathway acting downstream of cytochrome P450 oxidoreductase in skeletal development of the limb. *Mol Cell Biol* 2009, *29*, 2716-2729.

[11] Simonaro, C. M., Sachot, S., Ge, Y., He, X., *et al.*, Acid ceramidase maintains the chondrogenic phenotype of expanded primary chondrocytes and improves the chondrogenic differentiation of bone marrow-derived mesenchymal stem cells. *PLoS One* 2013, *8*, e62715.

[12] Masuko, K., Murata, M., Suematsu, N., Okamoto, K., *et al.*, A metabolic aspect of osteoarthritis: lipid as a possible contributor to the pathogenesis of cartilage degradation. *Clin Exp Rheumatol* 2009, *27*, 347-353.

[13] Mishra, R., Singh, A., Chandra, V., Negi, M. P., *et al.*, A comparative analysis of serological parameters and oxidative stress in osteoarthritis and rheumatoid arthritis. *Rheumatol Int* 2012, *32*, 2377-2382.

[14] Kosinska, M. K., Liebisch, G., Lochnit, G., Wilhelm, J., *et al.*, A lipidomic study of phospholipid classes and species in human synovial fluid. *Arthritis Rheum* 2013, *65*, 2323-2333.

[15] Zhou, X., Mao, J., Ai, J., Deng, Y., *et al.*, Identification of plasma lipid biomarkers for prostate cancer by lipidomics and bioinformatics. *PLoS One* 2012, *7*, e48889.

[16] Han, X., Rozen, S., Boyle, S. H., Hellegers, C., *et al.*, Metabolomics in early Alzheimer's disease: identification of altered plasma sphingolipidome using shotgun lipidomics. *PLoS One* 2011, *6*, e21643.

[17] Eriksson, C., Masaki, N., Yao, I., Hayasaka, T., Setou, M., MALDI Imaging Mass Spectrometry-A Mini Review of Methods and Recent Developments. *Mass Spectrom (Tokyo)* 2013, *2*, S0022.

[18] Cicione, C., Diaz-Prado, S., Muinos-Lopez, E., Hermida-Gomez, T., Blanco, F. J., Molecular profile and cellular characterization of human bone marrow mesenchymal stem cells: donor influence on chondrogenesis. *Differentiation* 2010, *80*, 155-165.

[19] Hermida-Gomez, T., Fuentes-Boquete, I., Gimeno-Longas, M. J., Muinos-Lopez, E., *et al.*, Bone marrow cells immunomagnetically selected for CD271+ antigen promote in vitro the repair of articular cartilage defects. *Tissue Eng Part A* 2011, *17*, 1169-1179.

[20] Rocha, B., Calamia, V., Mateos, J., Fernández-Puente, P., *et al.*, Metabolic labeling of human bone marrow mesenchymal stem cells for the quantitative analysis of their chondrogenic differentiation. *J Proteome Res* 2012, *11*, 5350-5361.

[21] Rocha, B., Calamia, V., Casas, V., Carrascal, M., *et al.*, Secretome analysis of human mesenchymal stem cells undergoing chondrogenic differentiation. *J Proteome Res* 2014, *13*, 1045-1054.

[22] Eijkel, G. B., Kaletas, B., Van der Wiel, I. M., Kros, J. M., *et al.*, Correlating MALDI and SIMS imaging mass spectrometric datasets of biological tissue surfaces. *Surf Interface* 2009, *41*, 675-685.

[23] Hoogerbrugge, R., Willig, S. J., Kistemaker, P. G., Discriminant analysis by double stage principal component analysis. *Anal Chem* 1983, *55*, 1710-1712.

[24] Petkovic, M., Schiller, J., Müller, M., Benard, S., *et al.*, Detection of individual phospholipids in lipid mixtures by matrix-assisted laser desorption/ionization time-of-flight mass spectrometry: phosphatidylcholine prevents the detection of further species. *Anal Biochem* 2001, *289*, 202-216.

[25] Chughtai, K., Jiang, L., Greenwood, T. R., Glunde, K., Heeren, R. M., Mass spectrometry images acylcarnitines, phosphatidylcholines, and sphingomyelin in MDA-MB-231 breast tumor models. *J Lipid Res* 2013, *54*, 333-344.

[26] Fletcher, J. S., Rabbani, S., Henderson, A., Blenkinsopp, P., *et al.*, A new dynamic in mass spectral imaging of single biological cells. *Anal Chem* 2008, *80*, 9058-9064.

[27] Carado, A., Passarelli, M. K., Kozole, J., Wingate, J. E., *et al.*, C60 secondary ion mass spectrometry with a hybrid-quadrupole orthogonal time-of-flight mass spectrometer. *Anal Chem* 2008, *80*, 7921-7929.

[28] Lanni, E. J., Rubakhin, S. S., Sweedler, J. V., Mass spectrometry imaging and profiling of single cells. *J Proteomics* 2012, *75*, 5036-5051.

[29] Jurchen, J. C., Rubakhin, S. S., Sweedler, J. V., MALDI-MS imaging of features smaller than the size of the laser beam. *J Am Soc Mass Spectrom* 2005, *16*, 1654-1659.

[30] Holle, A., Haase, A., Kayser, M., Höhndorf, J., Optimizing UV laser focus profiles for improved MALDI performance. *J Mass Spectrom* 2006, *41*, 705-716.

[31] Hankin, J. A., Barkley, R. M., Murphy, R. C., Sublimation as a method of matrix application for mass spectrometric imaging. *J Am Soc Mass Spectrom* 2007, *18*, 1646-1652.

[32] Schwamborn, K., Caprioli, R. M., MALDI imaging mass spectrometry--painting molecular pictures. *Mol Oncol* 2010, *4*, 529-538.

[33] Passarelli, M. K., Winograd, N., Lipid imaging with time-of-flight secondary ion mass spectrometry (ToF-SIMS). *Biochim Biophys Acta* 2011, *1811*, 976-990.

[34] Shimma, S., Sugiura, Y., Hayasaka, T., Hoshikawa, Y., *et al.*, MALDI-based imaging mass spectrometry revealed abnormal distribution of phospholipids in colon cancer liver metastasis. *J Chromatogr B Analyt Technol Biomed Life Sci* 2007, *855*, 98-103.

[35] Ide, Y., Waki, M., Hayasaka, T., Nishio, T., *et al.*, Human breast cancer tissues contain abundant phosphatidylcholine(36:1) with high stearoyl-CoA desaturase-1 expression. *PLoS One* 2013, *8*, e61204.

[36] Goto, T., Terada, N., Inoue, T., Nakayama, K., *et al.*, The expression profile of phosphatidylinositol in high spatial resolution imaging mass spectrometry as a potential biomarker for prostate cancer. *PLoS One* 2014, *9*, e90242.

[37] Cillero-Pastor, B., Eijkel, G. B., Kiss, A., Blanco, F. J., Heeren, R. M., Matrix-assisted laser desorption ionization-imaging mass spectrometry: a new methodology to study human osteoarthritic cartilage. *Arthritis Rheum* 2013, *65*, 710-720.

[38] Peffers, M. J., Cillero-Pastor, B., Eijkel, G. B., Clegg, P. D., Heeren, R. M., Matrix assisted laser desorption ionization mass spectrometry imaging identifies markers of ageing and osteoarthritic cartilage. *Arthritis Res Ther* 2014, *16*, R110.

[39] Malmberg, P., Jennische, E., Nilsson, D., Nygren, H., High-resolution, imaging TOF-SIMS: novel applications in medical research. *Anal Bioanal Chem* 2011, *399*, 2711-2718.

[40] Cillero-Pastor, B., Eijkel, G., Kiss, A., Blanco, F. J., Heeren, R. M., Time-of-flight secondary ion mass spectrometry-based molecular distribution distinguishing healthy and osteoarthritic human cartilage. *Anal Chem* 2012, *84*, 8909-8916.

[41] Malmberg, P., Nygren, H., Richter, K., Chen, Y., *et al.*, Imaging of lipids in human adipose tissue by cluster ion TOF-SIMS. *Microsc Res Tech* 2007, *70*, 828-835.

[42] Malmberg, P., Nygren, H., Methods for the analysis of the composition of bone tissue, with a focus on imaging mass spectrometry (TOF-SIMS). *Proteomics* 2008, *8*, 3755-3762.

[43] Steinhauser, M. L., Bailey, A. P., Senyo, S. E., Guillermier, C., *et al.*, Multi-isotope imaging mass spectrometry quantifies stem cell division and metabolism. *Nature* 2012, *481*, 516-519.

[44] Kokesch-Himmelreich, J., Schumacher, M., Rohnke, M., Gelinsky, M., Janek, J., ToF-SIMS analysis of osteoblast-like cells and their mineralized extracellular matrix on strontium enriched bone cements. *Biointerphases* 2013, *8*, 17.

[45] Merrill, A. H., Schmelz, E. M., Dillehay, D. L., Spiegel, S., *et al.*, Sphingolipids--the enigmatic lipid class: biochemistry, physiology, and pathophysiology. *Toxicol Appl Pharmacol* 1997, *142*, 208-225.

[46] Xu, F., Yang, C. C., Gomillion, C., Burg, K. J., Effect of ceramide on mesenchymal stem cell differentiation toward adipocytes. *Appl Biochem Biotechnol* 2010, *160*, 197-212.

[47] Jang, M. Y., Chun, S. I., Mun, C. W., Hong, K. S., Shin, J. W., Evaluation of metabolomic changes as a biomarker of chondrogenic differentiation in 3D-cultured human mesenchymal stem cells using proton (1H) nuclear magnetic resonance spectroscopy. *PLoS One* 2013, *8*, e78325.

Figure 1. **The spectra of all pellets collected at days 2 and 14 of chondrogenic differentiation after positive and negative matrix-assisted laser desorption ionization-mass spectrometry imaging (MALDI-MSI) were analyzed using principal component analysis (PCA) and discriminant analysis (DA) to classify specific lipids at each time point.** (A-B) Histogram distribution and spectra loading plot of first discriminant function (DF1) scores after positive ion MALDI-MSI measurements. DF1 negative scores are specific to day 2 samples and positive scores to day 14 samples. In the low mass range of the spectra, the phosphocholine head group (m/z 184.1) as well as a related ion at m/z 198.1 are primarily detected at day 2. The higher frequency of mass peaks at day 2 in the mass range from 680 to 860 indicates a higher content of PCs and SMs at this time point. (C-D) Histogram distribution and spectra loading plot of DF1 scores obtained after negative ion MALDI-MSI measurements. DF1 negative scores are specific to micromasses collected at day 14 and positive scores to day 2 samples. In addition to unsaturated fatty acids (m/z 303.2, m/z 327.2), many phosphatidylethanolamines (PEs) and phosphatidylinositols (PIs) are very abundant in MSC pellets from day 14.

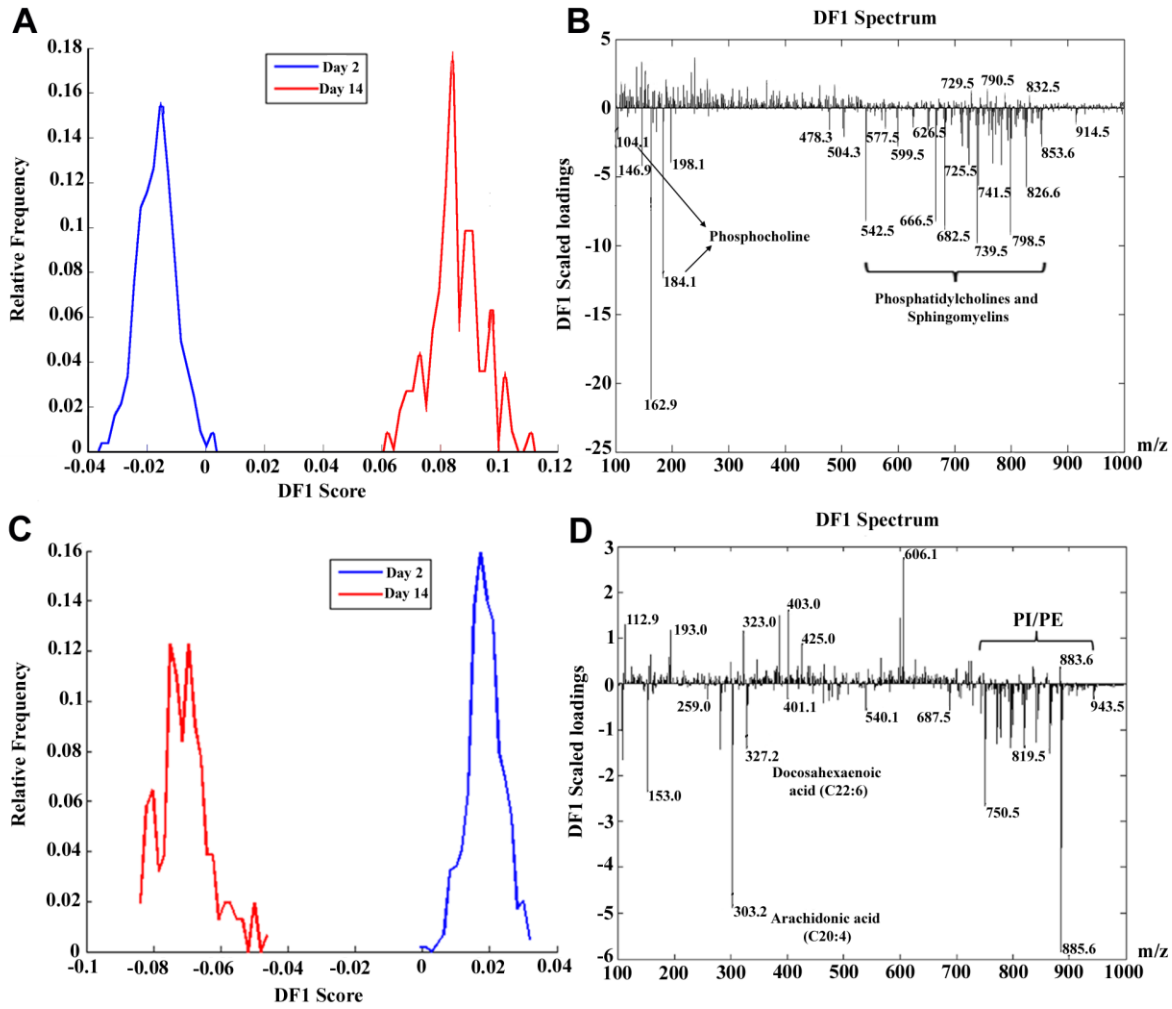

Figure 2. Spatial mapping of lipid-positive (A) and negative- (B) ions in micromass sections. (A) Distribution in ascending mass range of lipids ions: phosphocholine at m/z 184.1; a fragment from phosphatidylcholine (PC) (16:0/18:1) at m/z 504.3; fragments from sphingomyelin (SM) (d18:1/16:0) at m/z 542.5 and m/z 666.5; SM (d18:1/16:0-N$(CH_3)_3$ at m/z 682.5; and several PCs, PC (16:0/18:1) at m/z 782.6, PC (36:2) at m/z 824.5 and PC (18:0/18:1) at m/z 826.6, obtained after positive ion matrix-assisted laser desorption ionization-mass spectrometry imaging (MALDI-MSI) analysis and detected by time-of-flight secondary ion mass spectrometry (TOF-SIMS). (B) Distribution in ascending mass range of lipids ions: inositol monophosphate $[M-H]^-$ at m/z 259.0; arachidonic acid $[M-H]^-$ at m/z 303.2; docosahexaenoic acid $[M-H]^-$ at m/z 327.2; phosphatidylethanolamine (PE) (18:0/20:4) $[M-H]^-$ at 750.5; sulfatide (ST) (d18:1/16:0) $[M-H]^-$ at m/z 778.5; PE (18:0/22:4) $[M-H]^-$ at m/z 794.5; phosphatidylglycerol (PG) (18:1/22:6) at m/z 819.5; phosphatidylinositol (PI) (18:1/20:4) $[M-H]^-$ at m/z 883.6; PI (18:0/20:4) $[M-H]^-$ at m/z 885.6 and PI (42:3) $[M-H]^-$ at m/z 943.5. Scale bar show normalized intensities. Scale size 900 μm:

m/z= mass/charge.

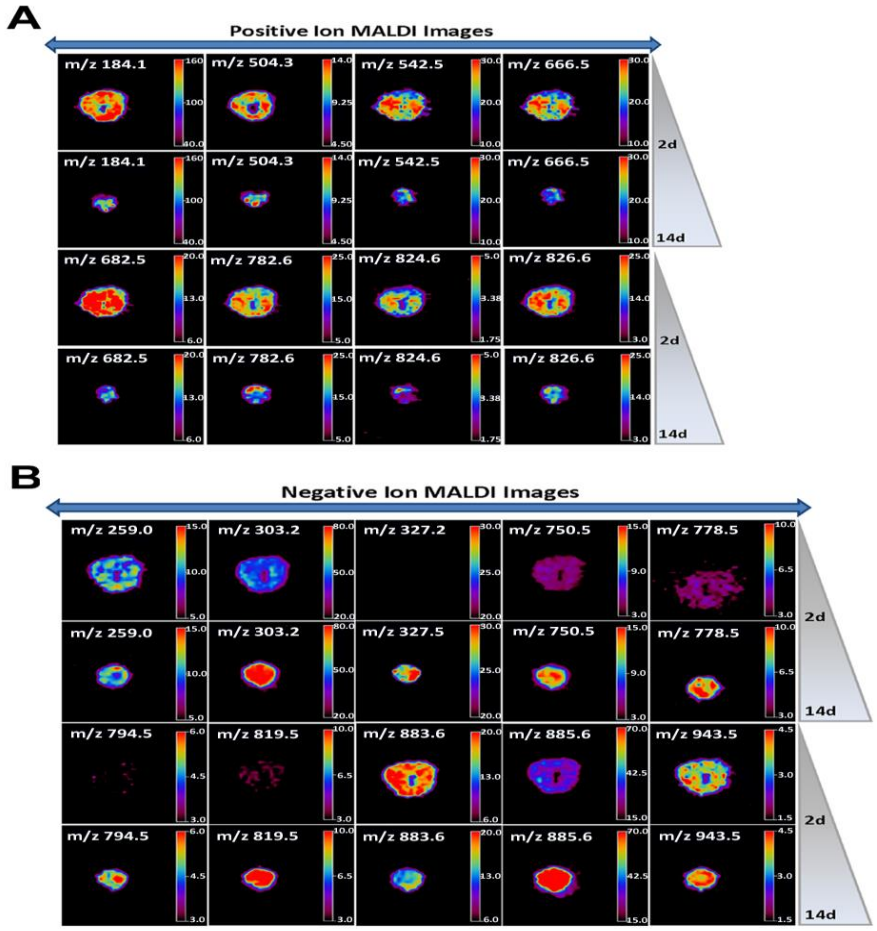

Figure 3. High spatial resolution time-of-flight secondary ion mass spectrometry (TOF-SIMS) imaging of choline and phosphocholine in day 2 and 14 micromass sections. Choline and phosphocholine are more abundant in the cells situated in the peripheral zone of the micromasses collected at day 14. The corresponding H&E staining images are also shown.

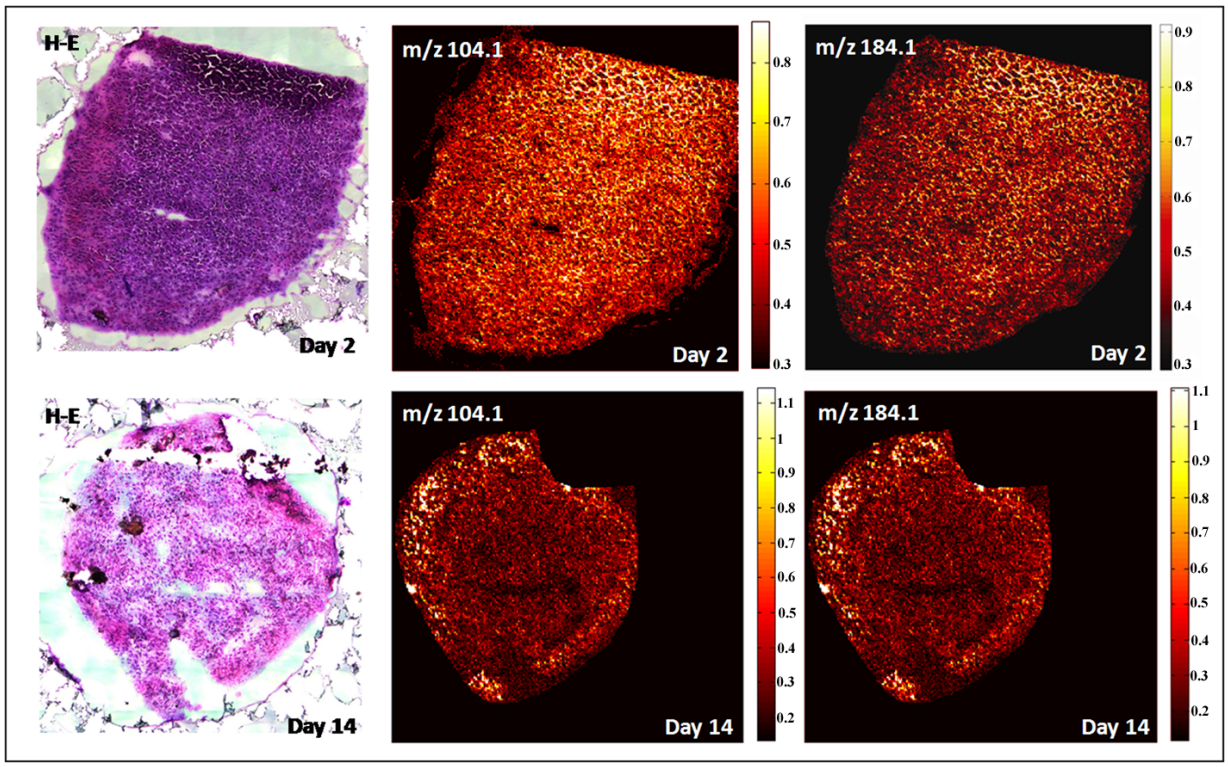

Figure 4. Enzymes involved in the sphingomyelin metabolism pathway are increased at day 14 of chondrogenesis. Expression of sphingomyelin phosphodiesterase (SMPD1), N-acylsphingosine amidohydrolase (ASAH1) and sphingosine kinase 1 (SPHK1) was quantified by RT-PCR. The results were normalized to the expression of the housekeeping gene RPL13 and are presented as the mean of six independent experiments in duplicate (*p <0.05relative to day 2). The SM pathway is illustrated at the top of the graphic. SM, sphingomyelin; S1P, sphingosine-1-phosphate.

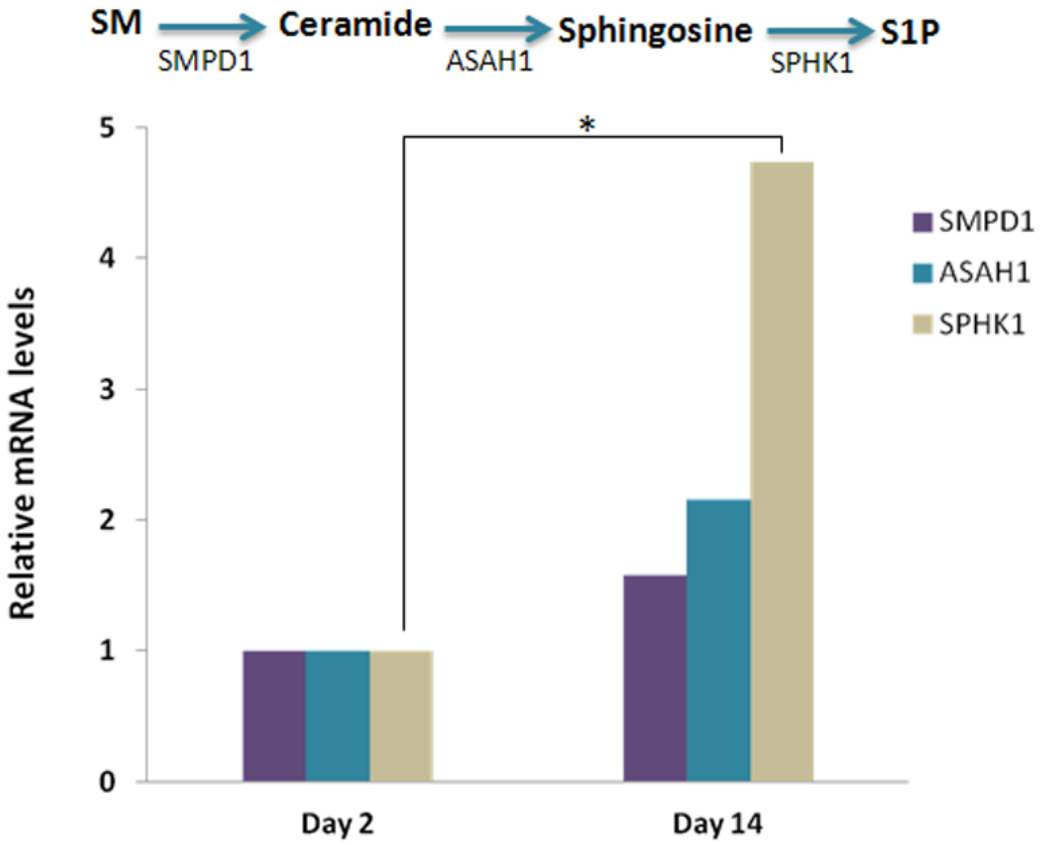

Tables

Table 1. Lipid profiles of hBMSCs undergoing chondrogenesis after MALDI-MSI analysis. The specific positive and negative m/z values, with the highest discriminant function loadings at days 2 and 14 of chondrogenic differentiation are summarized.

m/z value [a)]	Lipid assignment[b)]	Designation[c)]	Condition[d)]
104.1	Choline	$[M+H]^+$	Day 2
146.9	Sodiated headgroup of PC	$[M+Na]^+$	Day 2
153.0	Dehydrated phosphoglycerol	$[M-H]^-$	Day 14
162.9	Potassiated headgroup of PC	$[M+K]^+$	Day 2
184.1	Phosphocholine	$[M+H]^+$	Day 2
198.1	Phosphocholine-related ion	$[M+H]^+$	Day 2
259.0	Inositol monophosphate	$[M-H]^-$	Day 14
303.2	Arachidonic acid (C20:4)	$[M-H]^-$	Day 14
327.2	Docosahexaenoic acid (C22:6)	$[M-H]^-$	Day 14
478.3	Fragment from m/z PC (16:0/18:1)	$[M+K]^+$	Day 2
504.3	Fragment from m/z PC (16:0/18:1)	$[M+K]^+$	Day 2
542.5	Fragment from m/z SM (d18:1/16:0)	$[M+K]^+$	Day 2
577.5	Fragment from m/z PC (16:0/18:1)	$[M+K]^+$	Day 2
599.5	Fragment from m/z PC (16:0/18:1)	$[M+K]^+$	Day 2
666.5	Fragment from m/z SM (d18:1/16:0)	$[M+Na]^+$	Day 2
682.5	SM (d18:1/16:0-$N(CH_3)_3$	$[M+K]^+$	Day 2
723.5	SM (d18:1/16:1)	$[M+Na]^+$	Day 2
725.5	SM (d18:1/16:0)	$[M+Na]^+$	Day 2
729.5	SM (d18:1/18:1)	$[M+H]^+$	Day 14
739.5	PC (16:0/18:1-$N(CH_3)_3$	$[M+K]^+$	Day 2
741.5	SM (d18:1/16:0)	$[M+K]^+$	Day 2
750.5	PE (18:0/20:4)	$[M-H]^-$	Day 14
767.5	SM (d18:1/19:0) or SM(d18:1/18:1)	$[M+Na]^+$ or $[M+K]^+$	Day 2
778.5	ST (d18:1/16:0)	$[M-H]^-$	Day 14
782.6	PC (16:0/18:1)	$[M+Na]^+$	Day 2
790.5	PC (18:0/18:0)	$[M+H]^+$	Day 14
794.5	PE (18:0/22:4)	$[M-H]^-$	Day 14
798.5	PC (16:0/18:1)	$[M+K]^+$	Day 2
800.5	PC (34:0)	$[M+K]^+$	Day 2
819.5	PG (18:1/22:6)	$[M-H]^-$	Day 14

824.5	PC (36:2)	$[M+K]^+$	Day 2
826.6	PC (18:0/18:1)	$[M+K]^+$	Day 2
832.5	PC (18:4/20:0)	$[M+Na]^+$	Day 14
853.6	SM (d18:1/24:0)	$[M+K]^+$	Day 2
883.6	PI (18:1/20:4)	$[M-H]^-$	Day 2
885.6	PI (18:0/20:4)	$[M-H]^-$	Day 14
943.5	PI (42:3)	$[M-H]^-$	Day 14

hBMSCs: human bone marrow mesenchymal stem cells; MALDI-MSI: matrix-assisted laser desorption ionization-mass spectrometry imaging; PC: phosphatidylcholine, SM: sphingomyelin, PE: phosphatidylethanolamine, ST: sulfatide, PG: phosphatidylglycerol and PI: phosphatidylinositol.

[a] m/z values identified after tandem mass spectrometry (MS/MS) analysis.

[b] Assignments of m/z values according to MS/MS analysis, bibliography and Lipimaps.org database.

[c] Adduct ions observed in the collision-induced dissociation (CID) mass spectrum.

[d] Chondrogenic time point at which the lipid species are mainly expressed.

Table 2. Lipid profiles of hBMSCs undergoing chondrogenesis after TOF-SIMS analysis.

m/z value[a)]	Lipid assignment[b)]	Condition
184.1	Phosphocholine	Day 2
313.4	MAG (16:0)	Day 14
339.4	MAG (18:1)	Day 14
341.4	MAG (18:0)	Day 14
504.3	Fragment from m/z PC (16:0/18:1)	Day 2
542.5	Fragment from m/z SM (d18:1/16:0)	Day 2
551.6	DAG (32:0)	Day 14
575.7	DAG (34:2)	Day 14
576.7	Cer (d18:1/20:0)	Day 14
579.7	DAG (34:0)	Day 14
603.7	DAG (36:2)	Day 14
604.8	Cer (d18:1/22:0)	Day 14
605.7	DAG (36:1)	Day 14
607.8	DAG (36:0)	Day 14
666.5	Fragment from m/z SM (d18:1/16:0)	Day 2
682.5	SM (d18:1/16:0-N$(CH_3)_3$	Day 2
782.6	PC (16:0/18:1)	Day 2
824.5	PC (36:2)	Day 2
826.6	PC (18:0/18:1)	Day 2

hBMSCs: human bone marrow mesenchymal stem cells; TOF-SIMS: time-of-flight secondary ion mass spectrometry; PC: phosphatidylcholine, SM: sphingomyelin, MAG: monoacylglycerol, DAG: diacylglycerol, Cer: Ceramide.

a) m/z values with the highest discriminant function loadings selected after discriminant analysis (DA).

b) Tentative assignments according to the Lipidmaps.org database and lipid literature.

Supporting Information

Supplementary Figure 1. Experimental workflow for the characterization of lipids in micromasses by matrix-assisted laser desorption ionization-mass spectrometry imaging (MALDI-MSI) and time-of-flight secondary ion mass spectrometry (TOF-SIMS). Micromasses collected at day 2 and 14 of chondrogenesis were gelatin-embedded and cryo-sectioned into 10 µm sections for MSI. For (positive and negative) MALDI-MSI experiments, samples were sprayed with matrix using ImagePrep and analyzed to obtain lipid profiles. TOF-SIMS was then performed on gold-coated sections, providing high spatial resolution images of samples. Statistical methods used for data interpretation were principal component analysis (PCA) and discriminant analysis (DA). Lipid ion images were generated with Biomap 3.7.5.5 software. Lipids were identified by MALDI-tandem mass spectrometry (MALDI-MS/MS) profiling experiments performed directly on micromass sections.

Supplementary Figure 2. Discriminant Analysis (DA) confirms the lipid profile reproducibility among three human donors of bone marrow mesenchymal stem cells (hBMSCs) after positive ion matrix-assisted laser desorption ionization-mass spectrometry imaging (MALDI-MSI) experiments. (A) Histogram distribution of first discriminant function (DF1) scores. **(B)** Spectra loading plot of the DF1. The negative part of the spectrum corresponds to micromasses collected at day 2 of chondrogenesis and shows a higher content of phosphatidylcholines (PCs) and sphingomyelins (SMs) compared with samples from day 14.

Supplementary Figure 3. Distribution and intensities of lipid positive ions in micromass sections after matrix-assisted laser desorption ionization-mass spectrometry imaging (MALDI-MSI) experiments and tandem mass spectrometry

(MS/MS) profiling identifications. Scale bars show normalized intensities. Scale size: 900 μm:

Supplementary Figure 4. Representative fragmentation spectra of some phospholipid and sphingolipid molecular ions detected from micromasses in positive and negative ion mode analyses. (A) Tandem mass spectrometry (MS/MS) spectrum and structure of sphingomyelins (SM) (d18:1/16:0). The ion at m/z 86 is a specific fragment of the choline head group. The neutral loss of the entire phosphocholine head group led to the formation of the fragment ion $[M+H-183]^+$ at m/z 542.5 from the sodiated-SM precursor, whereas the loss of trimethylamine from the phosphocholine head group generated the fragment ion $[M+H-59]^+$ at m/z 666.5. **(B)** MS/MS spectrum and structure of phosphatidylcholine (PC) (16:0/18:1-$N(CH_3)_3$. The fragment ions at m/z 483.2 and m/z 456.2 correspond to the loss of the 16:0 and 18:1 fatty acid chain from the potassiated-PC precursor. **(C)** MS/MS spectrum and structure of phosphatidylglycerol (PG) (18:1/22:6). **(D)** MS/MS spectra of phosphatidylinositol (PI) (18:0/20:4). The mass peaks at m/z 241 (inositolphosphate-H_2O) and 223 (inositolphosphate-$2H_2O$) confirm the presence of the inositol polar head group. The assignment of the fatty acid chains was confirmed by the mass peaks at m/z 581 and m/z 601, which are characteristic of the loss of the arachidonic and stearic acid, respectively. The fragment ion at m/z 419 is related to the loss of the inositol headgroup (162 Da) plus the C18:0 fatty acid

Figure 1:

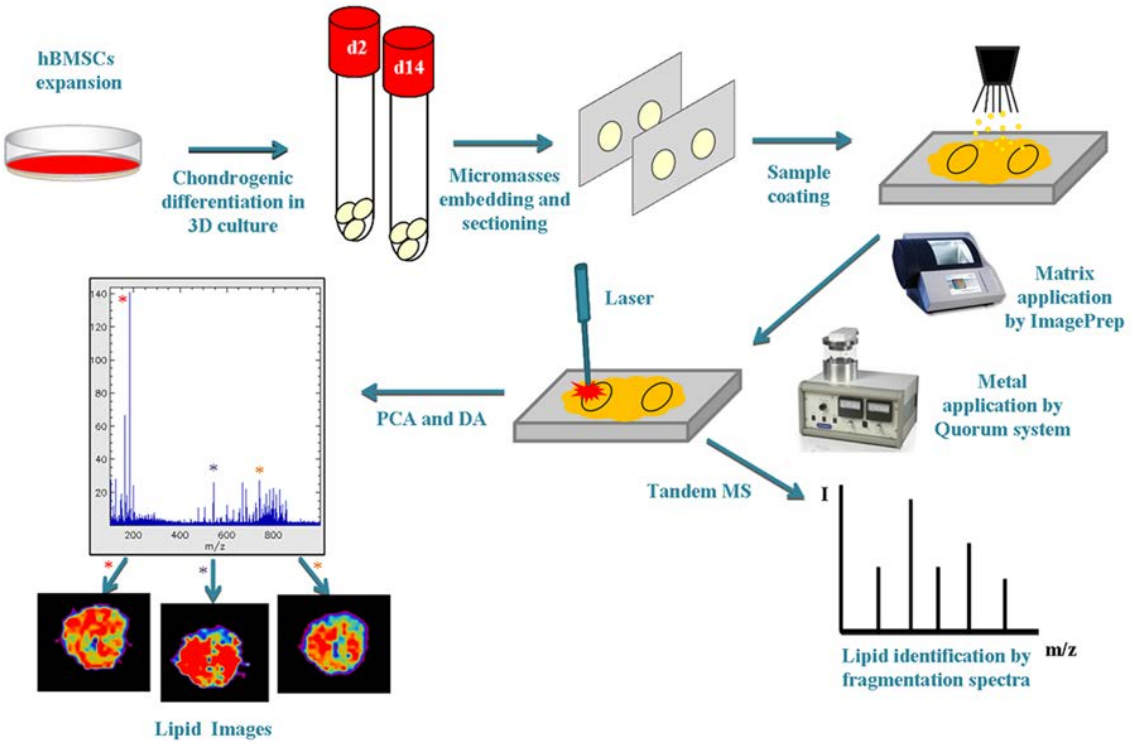
hBMSCs expansion
Chondrogenic differentiation in 3D culture
d2
d14
Micromasses embedding and sectioning
Sample coating
Matrix application by ImagePrep
Metal application by Quorum system
Laser
PCA and DA
Tandem MS
I
m/z
Lipid identification by fragmentation spectra
Lipid Images

Figure 2:

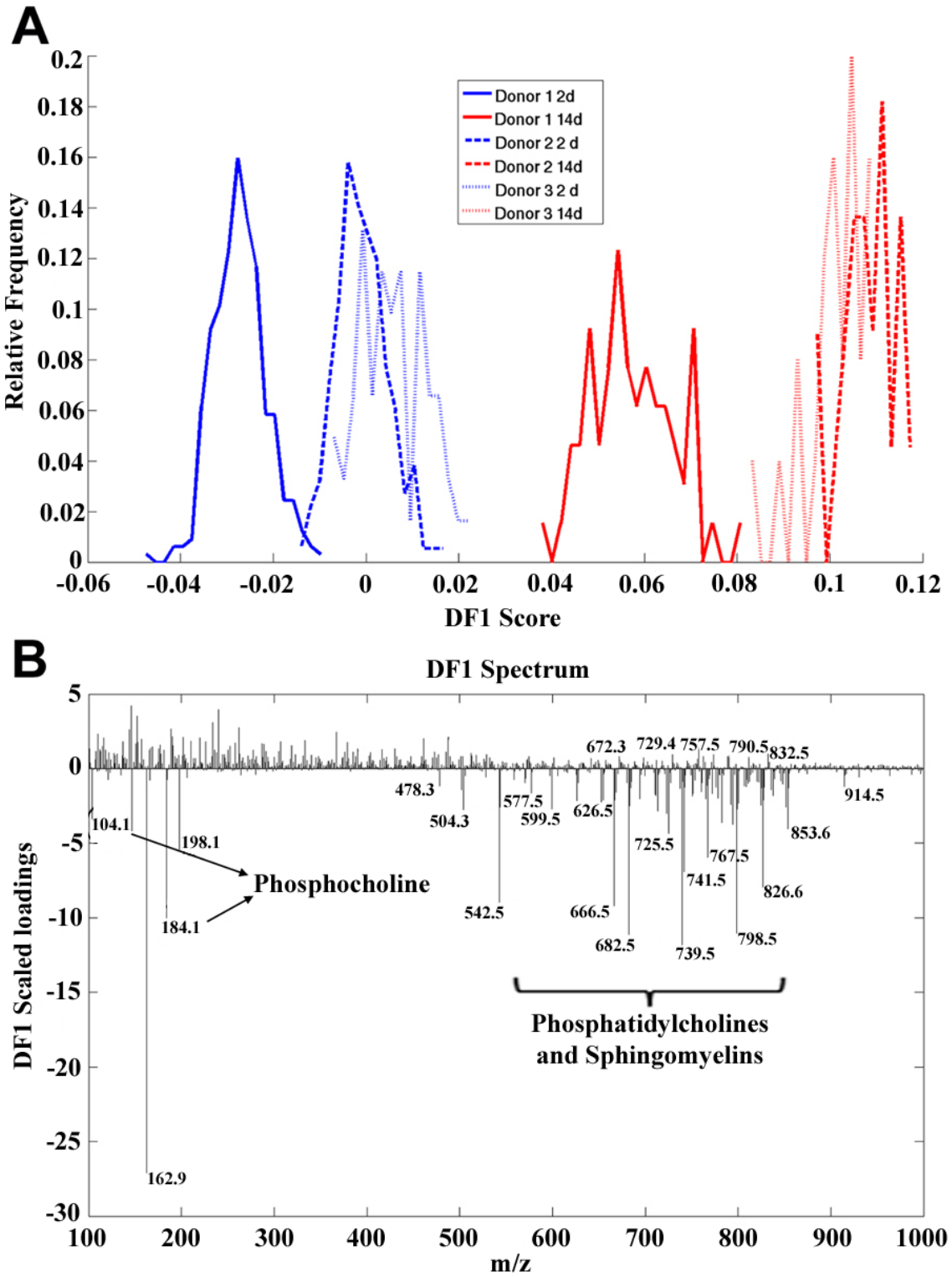
A
Donor 1 2d
Donor 1 14d
Donor 2 2 d
Donor 2 14d
Donor 3 2 d
Donor 3 14d
Relative Frequency
DF1 Score
B
DF1 Spectrum
DF1 Scaled loadings
m/z
104.1
198.1
184.1
162.9
Phosphocholine
478.3
504.3
542.5
577.5
599.5
626.5
666.5
672.3
682.5
729.4
725.5
739.5
757.5
741.5
767.5
790.5
798.5
826.6
832.5
853.6
914.5
Phosphatidylcholines
and Sphingomyelins

Figure 3:

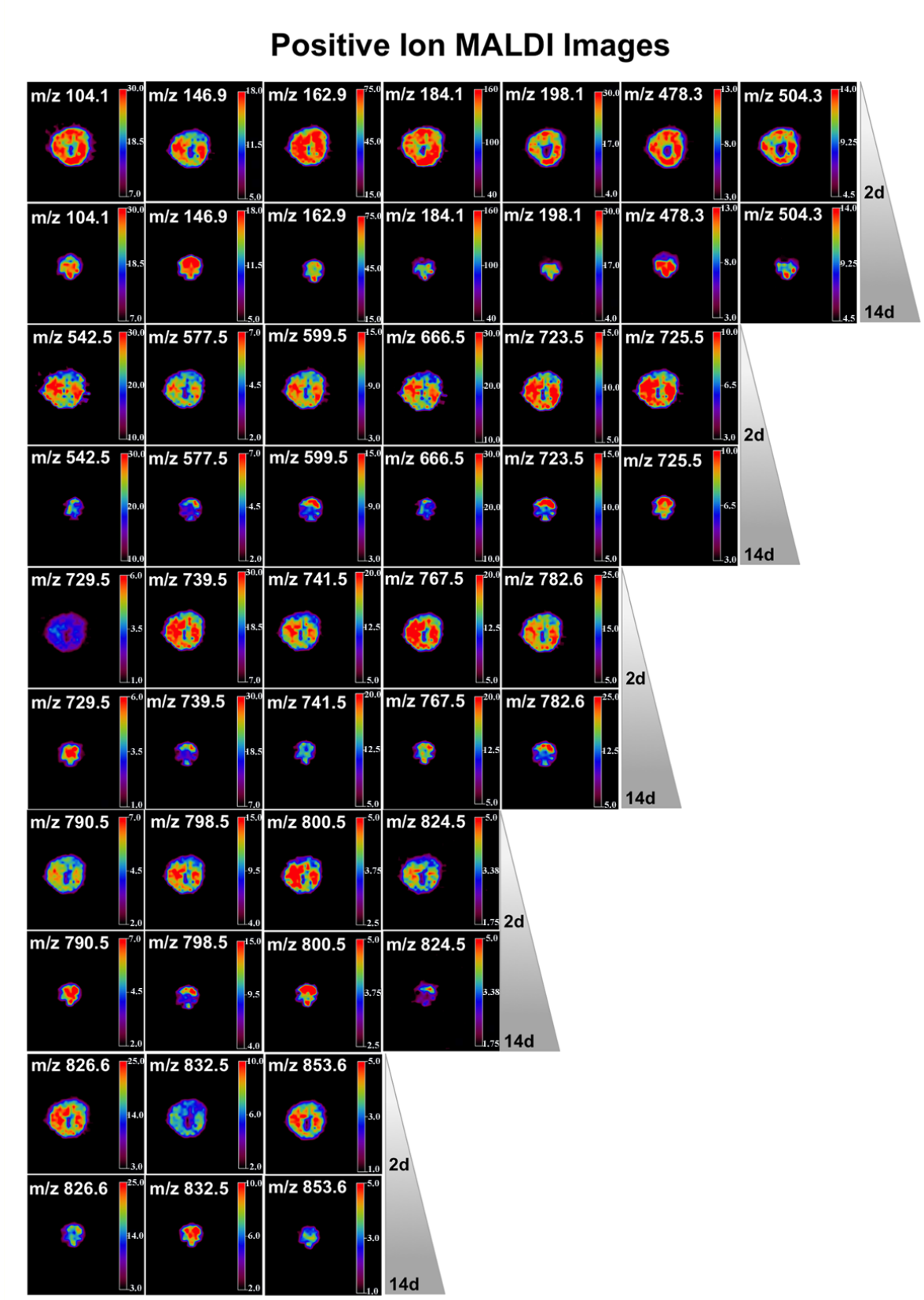
Positive Ion MALDI Images
m/z 104.1
m/z 146.9
m/z 162.9
m/z 184.1
m/z 198.1
m/z 478.3
m/z 504.3
2d
m/z 104.1
m/z 146.9
m/z 162.9
m/z 184.1
m/z 198.1
m/z 478.3
m/z 504.3
14d
m/z 542.5
m/z 577.5
m/z 599.5
m/z 666.5
m/z 723.5
m/z 725.5
2d
m/z 542.5
m/z 577.5
m/z 599.5
m/z 666.5
m/z 723.5
m/z 725.5
14d
m/z 729.5
m/z 739.5
m/z 741.5
m/z 767.5
m/z 782.6
2d
m/z 729.5
m/z 739.5
m/z 741.5
m/z 767.5
m/z 782.6
14d
m/z 790.5
m/z 798.5
m/z 800.5
m/z 824.5
2d
m/z 790.5
m/z 798.5
m/z 800.5
m/z 824.5
14d
m/z 826.6
m/z 832.5
m/z 853.6
2d
m/z 826.6
m/z 832.5
m/z 853.6
14d

Figure 4:

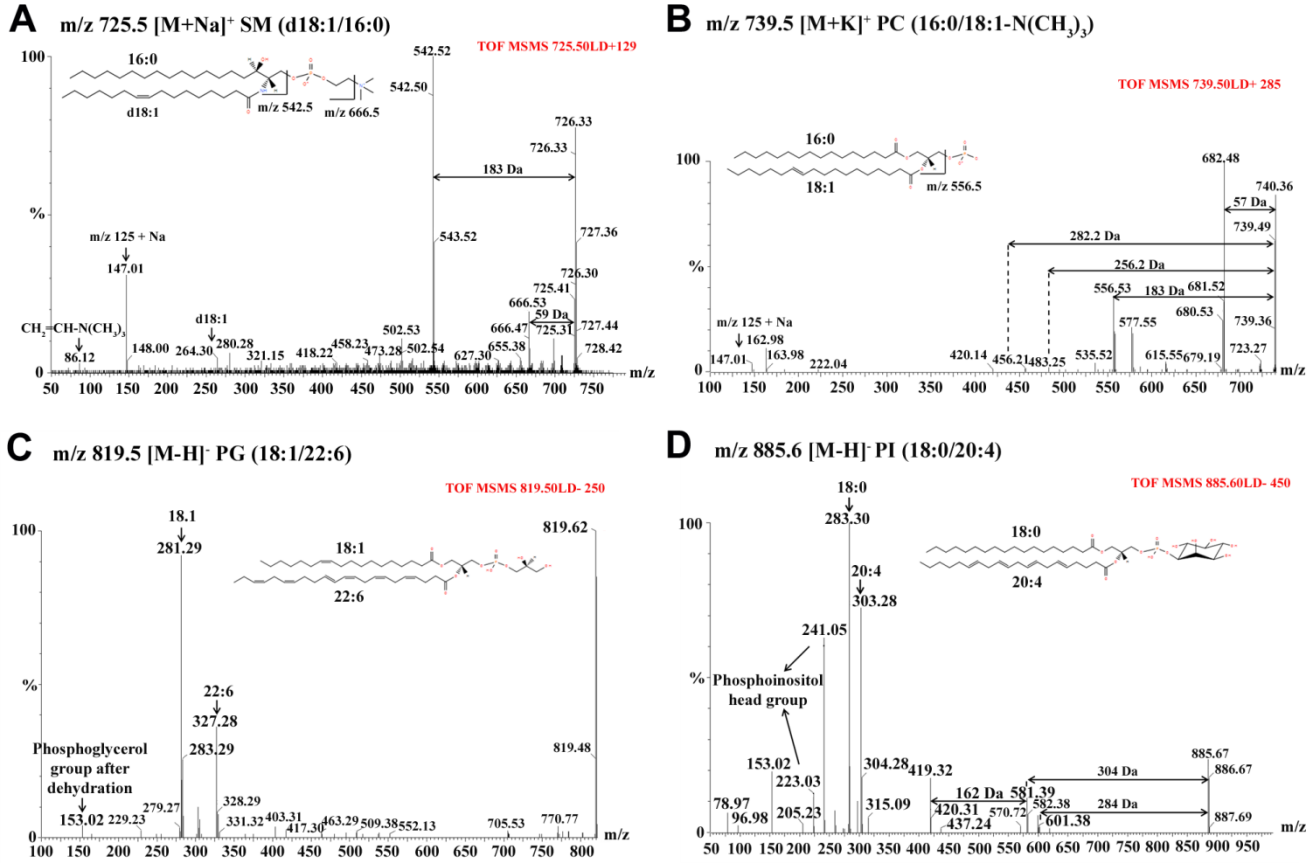
A
m/z 725.5 [M+Na]+ SM (d18:1/16:0)
TOF MSMS 725.50LD+129
16:0
d18:1
m/z 542.5
m/z 666.5
542.52
542.50
726.33
726.33
183 Da
m/z 125 + Na
147.01
543.52
727.36
726.30
725.41
666.53
59 Da
CH2=CH-N(CH3)3
86.12
d18:1
148.00
264.30
280.28
321.15
418.22
458.23
473.28
502.53
502.54
627.30
666.47
725.31
655.38
727.44
728.42
m/z
B
m/z 739.5 [M+K]+ PC (16:0/18:1-N(CH3)3)
TOF MSMS 739.50LD+ 285
16:0
18:1
m/z 556.5
682.48
740.36
57 Da
739.49
282.2 Da
256.2 Da
556.53
183 Da
681.52
680.53
577.55
739.36
m/z 125 + Na
162.98
147.01
163.98
222.04
420.14
456.21
483.25
535.52
615.55
679.19
723.27
m/z
C
m/z 819.5 [M-H]- PG (18:1/22:6)
TOF MSMS 819.50LD- 250
18.1
281.29
18:1
22:6
819.62
22:6
327.28
Phosphoglycerol
group after
dehydration
283.29
819.48
153.02
229.23
279.27
328.29
331.32
403.31
417.30
463.29
509.38
552.13
705.53
770.77
m/z
D
m/z 885.6 [M-H]- PI (18:0/20:4)
TOF MSMS 885.60LD- 450
18:0
283.30
20:4
303.28
18:0
20:4
241.05
Phosphoinositol
head group
153.02
223.03
304.28
419.32
885.67
304 Da
886.67
162 Da
581.39
78.97
96.98
205.23
315.09
420.31
437.24
570.72
582.38
284 Da
601.38
887.69
m/z